Supplementary Information

Quantum Metric Third-Order Nonlinear Hall Effect in A Non-Centrosymmetric Ferromagnet

Hao Yu[1], Ya-Qing Bie[1, 2], Peng Yu[1]*, Guowei Yang[1]

[1]*State Key Laboratory of Optoelectronic Materials and Technologies*, *Guangzhou Key Laboratory of Flexible Electronic Materials and Wearable Devices, Nanotechnology Research Center, School of Materials Science and Engineering, Sun Yat-sen University, Guangzhou 510275, P.R. China*

[2]*School of Electronics and Information Technology, Sun Yat-sen University, Guangzhou 510275, P.R. China*

*E-mail: yupeng9@mail.sysu.edu.cn

This file contains Supplemental Figures S1-S13 and Notes 1-12.

Note 1: Optical image of sub-centimeter level Fe_5GeTe_2 single crystal**.**

Note 2: SEM&EDS characterization of Fe_5GeTe_2.

Note 3: SHG characterization of Fe_5GeTe_2.

Note 4: Raman characterization of Fe_5GeTe_2.

Note 5: Sample thickness of the Fe_5GeTe_2 device in Fig. 4.

Note 6: *I*-*V* curve measured by 2-probe measurement.

Note 7: Effect of driving frequency in third order nonlinear Hall signal.

Note 8: Fe_5GeTe_2 device with different patterns of electrodes.

Note 9: First-harmonic V_{xxy}^{ω} as a function of V_{xx}^{ω} at temperature range from 80 to 400 K.

Note 10: The $V_{xxx}^{3\omega}$ signal as a function of the V_{xx}^{ω} at different temperatures from 80 to 400 K.

Note 11: Nonlinear transport testing of Fe_5GeTe_2 device (> 100 nm) at temperatures range from 1.6 to 300 K.

Supplemental Note 1: Optical image of sub-centimeter level Fe_5GeTe_2 single crystal.

By regulating the temperature and degree of vacuum in the reaction environment, in conjunction with the solid-state synthesis method of quenching to conclude the reaction, we were able to successfully prepare a high-quality Fe_5GeTe_2 single crystal with high crystallinity and good orientation. The single-crystal size, which is close to the centimeter level, has provided a solid foundation for the subsequent process.

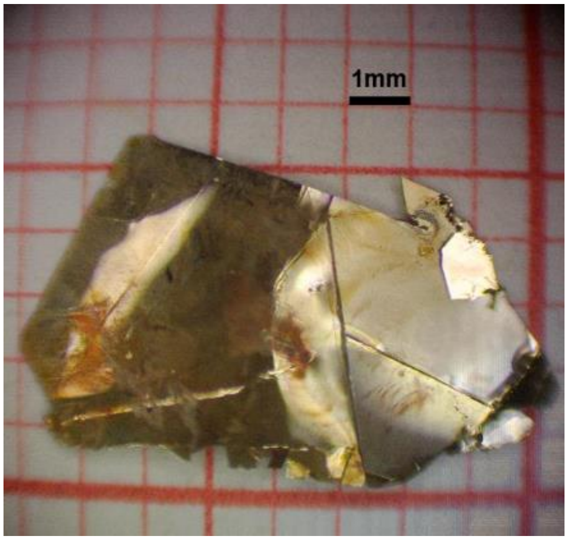

Supplementary Figure S1 |Optical image of Fe_5GeTe_2 single crystal.

Supplemental Note 2: SEM&EDS characterization of Fe_5GeTe_2.

Semi-quantitative microprobe analyses were conducted on single crystals of Fe_5GeTe_2 using a field emission scanning electron microscope (Hitachi SU8010) equipped with an energy dispersive X-ray spectroscope (EDX, IXRF). The energy dispersive spectra (EDS) obtained from the surface of the sample confirmed the presence of Fe, Ge, and Te elements, as illustrated in Figures S2 and S3.

Elemental analysis of materials is conducted using the direct analytical technique of energy dispersive X-ray spectroscopy (EDX). In order to obtain a clean surface for analysis, the samples are placed on a metal holder and exfoliated using tape prior to measurement. The EDX spectrum confirms the presence of the elements Fe, Ge and Te, with the formula $Fe_{5.4}Ge_1Te_{1.9}$.

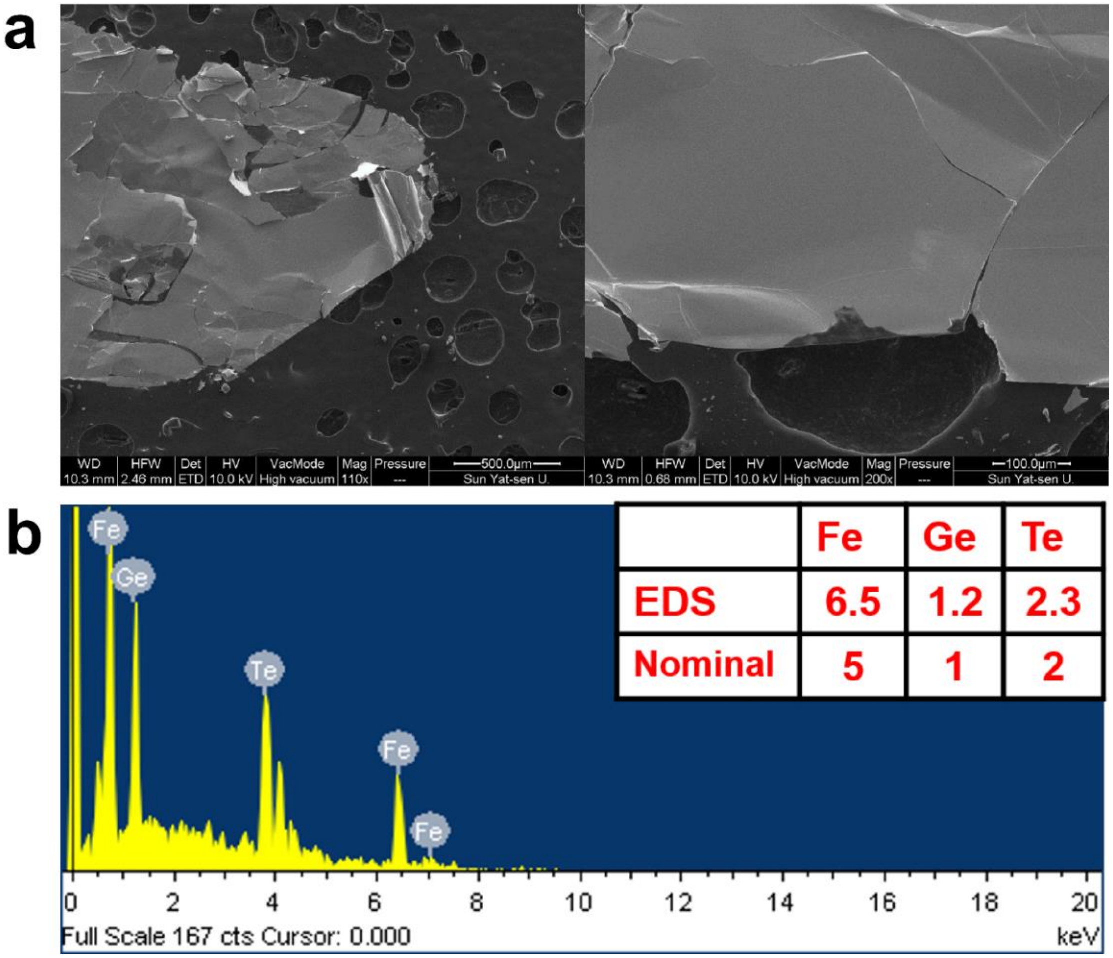

	Fe	Ge	Te
EDS	6.5	1.2	2.3
Nominal	5	1	2

Supplementary Figure S2 |a, Scanning electron microscope (SEM) image of Fe_5GeTe_2 crystals. b, The energy dispersive X-ray spectrum (EDS) result for Fe_5GeTe_2 crystals.

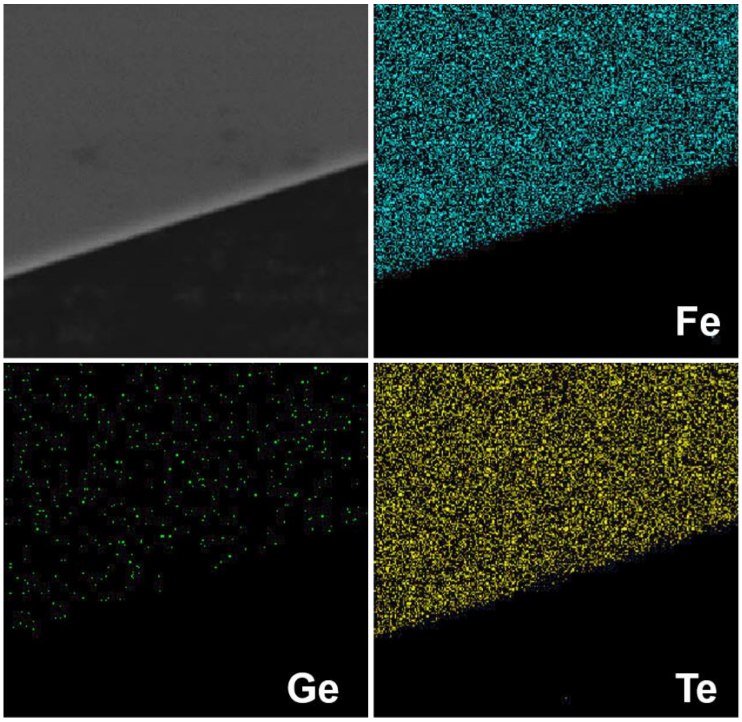

Supplementary Figure S3 |EDS elemental mapping for a typical Fe_5GeTe_2 flake. blue: Fe, green: Ge, yellow: Te.

Supplemental Note 3: SHG characterization of Fe_5GeTe_2.

The generation of second harmonic (SHG) is the most direct means to determine the centrosymmetric of two-dimensional materials. It is evident from SHG mapping that the Fe_5GeTe_2 exhibits a uniform distribution of SHG signal within the sample (Figure S4b), indicating the manifestation of inversion symmetry breaking.

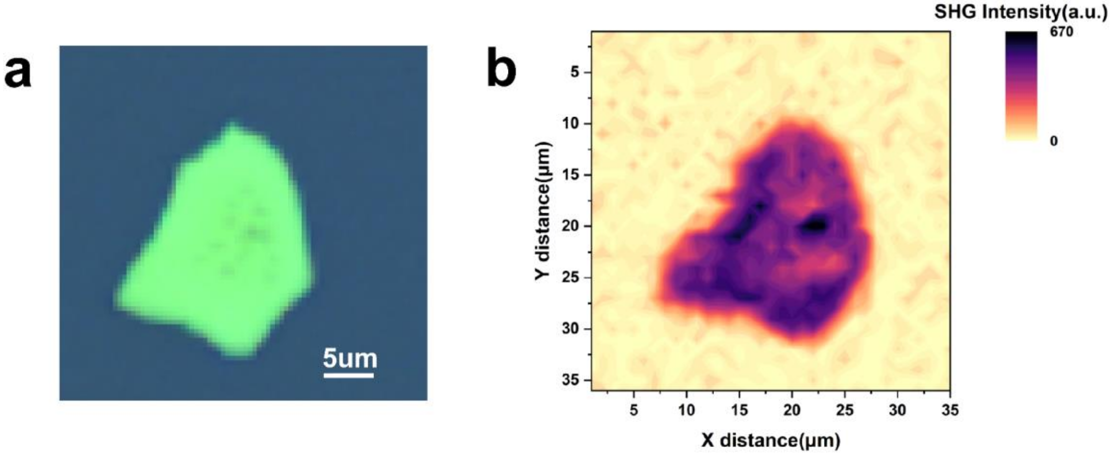

Supplementary Figure S4 |SHG characterization of Fe_5GeTe_2. a, Optical image of Fe_5GeTe_2 sample. b, SHG mapping image of Fe_5GeTe_2 sample.

Supplemental Note 4: Raman characterization of Fe_5GeTe_2.

Theoretically, the Raman scattered intensity can be described as:

$$I \propto |\langle e_i|R|e_s\rangle|^2 \tag{1}$$

where e_i and e_s sign the unit vector of the incident and scattered radiation, and R is the Raman tensor for a certain vibration mode. For $R3m$ space group in layered ferromagnetism Fe_5GeTe_2, the Raman tensors are presented in the following matrix:

$$R_{Az} = \begin{pmatrix} a & 0 & 0 \\ 0 & a & 0 \\ 0 & 0 & b \end{pmatrix} \quad R_{Ex} = \begin{pmatrix} c & d & e \\ d & -c & f \\ e & f & 0 \end{pmatrix}$$

$$R_{Ey} = \begin{pmatrix} d & -c & -f \\ -c & -d & e \\ -f & e & 0 \end{pmatrix} \tag{2}$$

where a, b, c, d, e and f are the tensor elements determined by the cross section of Raman scattering. In accordance with Equations (1) and (2), the Angle-dependent intensity for each mode can be expressed as follows:

$$I_{Az} \propto a^2 \tag{3}$$

$$I_{Ex} \propto (d^2+c^2)sin^2\,(2\theta + \varphi_1)\,,\ \varphi_1 = arcsin(\frac{c}{\sqrt{d^2+c^2}}) \tag{4}$$

$$I_{Ey} \propto (d^2+c^2)sin^2\,(2\theta - \varphi_2)\,,\ \varphi_2 = arcsin(\frac{d}{\sqrt{d^2+c^2}}) \tag{5}$$

where θ is the rotation angle of the sample. The results show that A_z, E_x and E_y modes have nonzero intensity. Moreover, The A_z mode is cyclic and the intensities of the E_x and E_y modes are proportional to a four-fold symmetric polynomial, which is in agreement with experimental measurements.

Raman spectroscopy was employed to analyze Fe_5GeTe_2 on a HORIBA Scientific Raman microscopy system with spectral resolution below 1 cm^{-1} under the illumination of a 532 nm laser. The Raman spectroscopy of Fe_5GeTe_2 exhibited two notable Raman peaks between 100 cm^{-1} and 150 cm^{-1}, which corresponded to A_z *and* E_y Raman vibrational modes. Furthermore, Raman spectra were measured at different polarized angles (Fig. 2c), demonstrating it Raman vibrational anisotropy. The intensities of the A_z Raman vibrational modes at different polarized angles were extracted and plotted in polar coordinates, where a normal circle (Figure S5a). A four-petal pattern (Figure S5b) were observed in the *E* Raman vibrational modes. However, the experiment does not effectively determine the direction of vibration in *E* mode. The Raman peak value of the bulk Fe_5GeTe_2 model was identified using density functional perturbation theory (DFPT) (Figure S5c, d). The discrepancies in Raman shifts resulting from interlayer interactions in models with varying layer numbers are negligible when calculations are performed using the bulk periodicity model. Analysis of the phonon spectrum derived from computational results reveals that the Raman vibrational mode at 141 cm^{-1} is characterized as E_y.

The first-principle calculations were performed with the Vienna ab initio simulation package (VASP)[1], which utilized the generalized gradient approximation (GGA)[2,3] in the Perdew-Burke Ernzerhof (PBE) exchange-correlation functionals[4]. The plane-wave cutoff energy was set to be 400 eV, and a Γ-central 10 × 10 × 10 k-point was used in structural optimization. In the framework of DFPT, the features of phonon were carried out with PHONOPY code[5]. The ferromagnetic state was considered in calculations. The convergence criteria for energy and atom forces were chosen as 10^5 eV and 0.01 eV/Å, respectively.

The blue shift of A_z and E_y mode occurred with the decrease of sample thickness (Figure S5e). The full width at half maxima of the A_z Raman vibration exhibits minimal variation prior to 300 K, followed by a significant decrease at temperatures below 300 K (Figure S5f).

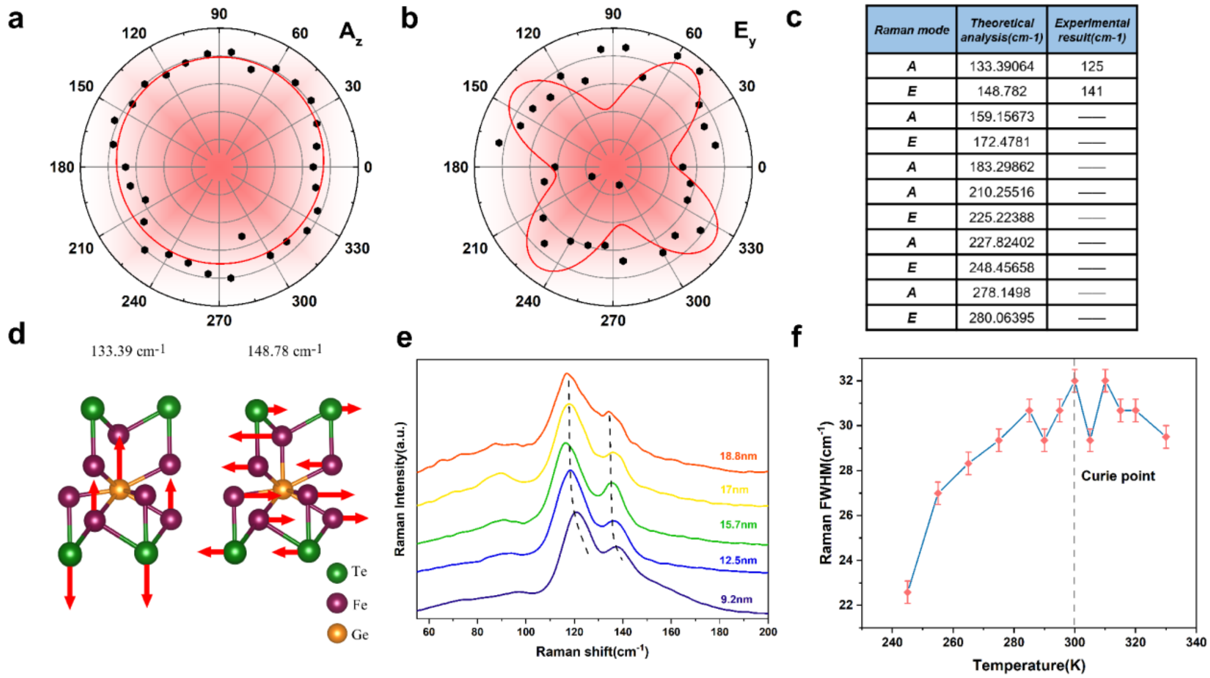

Raman mode	*Theoretical analysis(cm-1)*	*Experimental result(cm-1)*
A	133.39064	125
E	148.782	141
A	159.15673	——
E	172.4781	——
A	183.29862	——
A	210.25516	——
E	225.22388	——
A	227.82402	——
E	248.45658	——
A	278.1498	——
E	280.06395	——

Supplementary Figure S5|Raman characterization of Fe_5GeTe_2. a, b are polar plots of Raman intensity versus rotation angle for the A_z and E_y Raman active modes, respectively. c. Theoretical and experimental characteristics of the Raman active modes of Fe_5GeTe_2. d. Theoretical calculation of Raman vibration visualization model e. Raman spectra of varying thicknesses from 9.2 nm to 18.8 nm. f. The full width at half maxima the A_z Raman vibration as a function of temperature

Supplemental Note 5: Sample thickness of the Fe$_5$GeTe$_2$ device in Fig. 4.

Once the device has been prepared, the thickness of the device sample is determined through the Equation: d(h-BN+F$_5$GT) - d(h-BN) = d(F$_5$GT), in order to prevent oxidation of the sample.

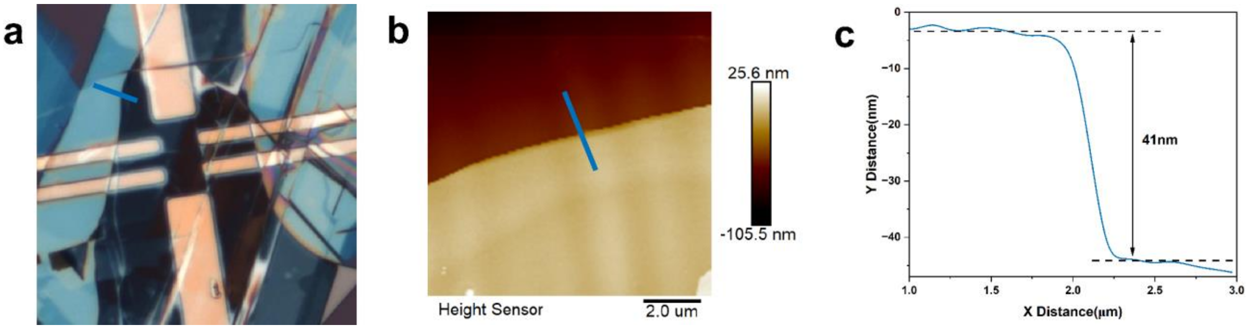

Supplementary Figure S6|Sample thickness of the Fe$_5$GeTe$_2$ device in Fig. 4 in the main text. a, Optical image of Fe$_5$GeTe$_2$ device b, AFM images of the Fe$_5$GeTe$_2$ device. c, Line profile of the corresponding position in (a).

Supplemental Note 6: *I-V* curve measured by 2-probe measurement.

Prior to commencing the DC *I-V* testing of the devices, it was first necessary to ascertain that they exhibited good linearity and symmetry (Figure S7). This was achieved, and it was thus established that the influence of the Schottky junction rectification effect on the test could be eliminated. Figure S7a illustrates that the resistance of *R*3*m* Fe$_5$GeTe$_2$ is isotropic, which is consistent with the text analysis. The design of the electrode layout results in a width of the transverse electrode in Figure S7b that is four times that of the longitudinal electrode. Therefore, the difference in *I-V* can be attributed to the channel area and contact area rather than to the anisotropy of resistance.

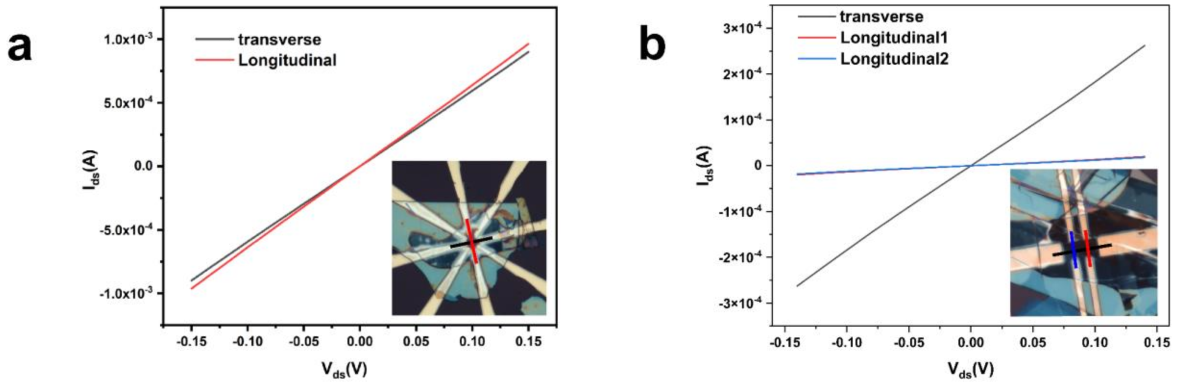

Supplementary Figure S7|2-probe measurement by a source meter. Linear *I-V* relationship is observed in the Fe_5GeTe_2 device. The *I-V* test plot for the device in Fig. 4 in the main text is shown on the right.

Supplemental Note 7: Effect of driving frequency in third order nonlinear Hall signal.

The third-order nonlinear Hall signal is independent of the driving frequency, which excludes possible artefacts from capacitive coupling.

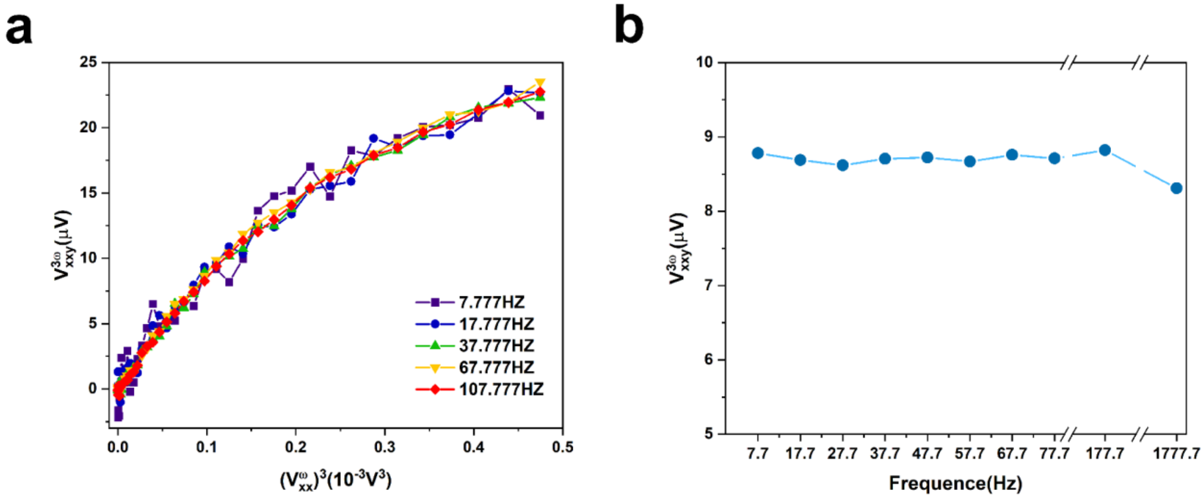

Supplementary Figure S8|Effect of driving frequency. a, The $V_{xxx}^{3\omega}$ signal as a function of the V_{xx}^{ω} at 300 K at different driving frequencies. b, The $V_{xxx}^{3\omega}$ signal is independent of driving frequencies when the device in Fig. 4 was injected with a constant V_{xx}^{ω} at 250 K.

Supplemental Note 8: Fe_5GeTe_2 device with different patterns of electrodes.

In order to eliminate the errors caused by certain factors, several devices with different electrode shapes were fabricated. These devices are capable of detecting third-order nonlinear Hall signals.

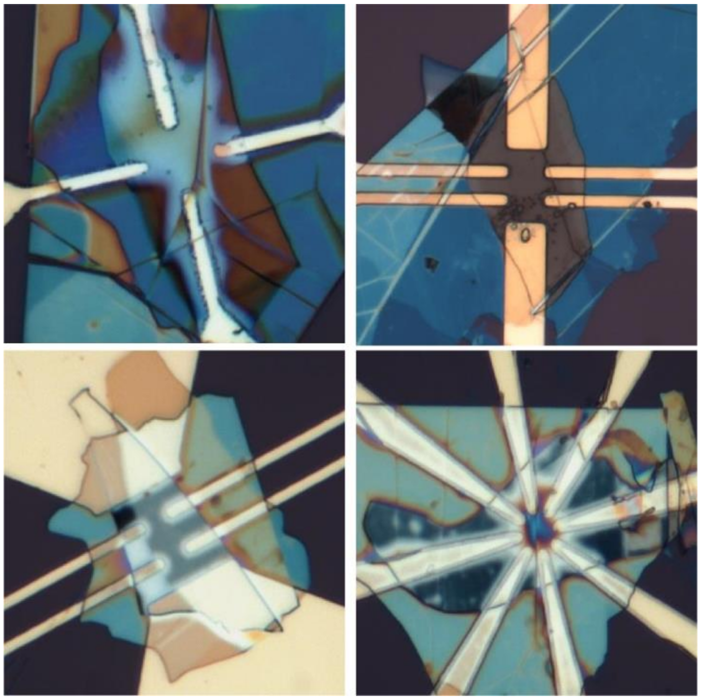

Supplementary Figure S9|Optical image of Fe_5GeTe_2 device with different patterns of electrodes.

Supplemental Note 9: First-harmonic V_{xxy}^{ω} as a function of V_{xx}^{ω} at temperature range from 80 to 400K.

In the absence of an applied magnetic field, the application of a transverse voltage to the device results in the detection of a hall longitudinal voltage (V_{xxy}^{ω}) that is linearly proportional to the transverse voltage (V_{xx}^{ω}). As C_{3V} in the text analysis eliminates Berry curvature to zero, it represents an ideal state. Consequently, the factors that induce the generation of the first-order signal are more complex, which may be attributed to the abnormal Hall effect induced by the built-in electron spin of Fe_5GeTe_2. As the ambient temperature is reduced, the intensity of the phenomenon in question increases.

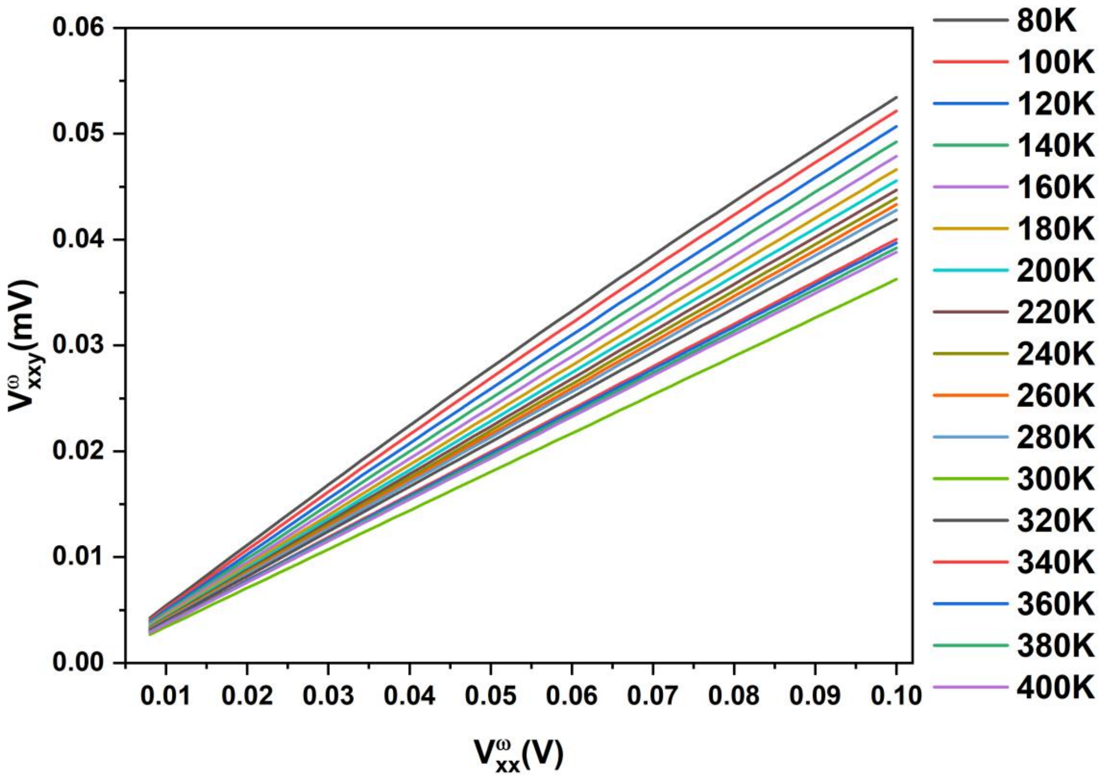

Supplementary Figure S10|First-harmonic V^{ω}_{xxy} as a function of V^{ω}_{xx} at temperature range from 80 to 400K.

Supplemental Note 10: Comparison of Second-order and Third-order signals in the same device.

The relative strength of the second-order and third-order signals in Fe_5GeTe_2 devices is compared under the same test environment of the same device. The third-order signals are approximately one order of magnitude larger than the second-order signals at different temperatures.

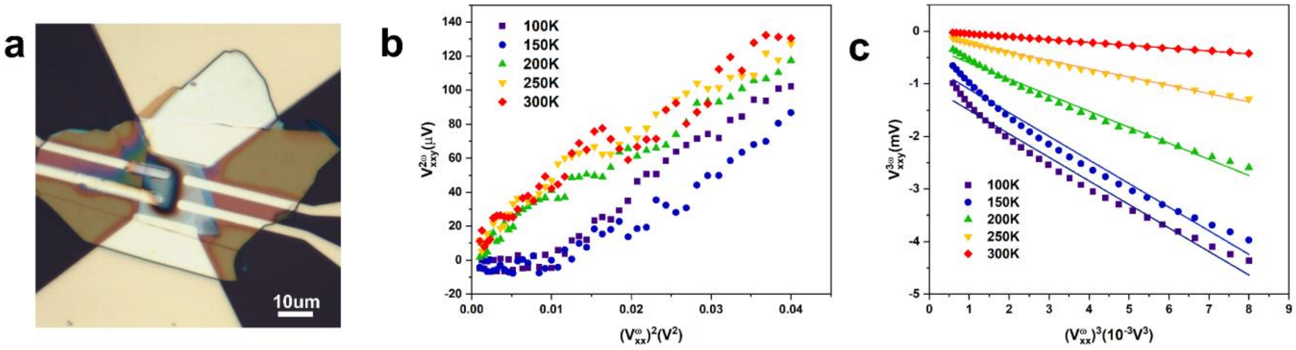

Supplementary Figure S11|Comparison of Second-order and Third-order signals in the same device. a, Optical image of Fe_5GeTe_2 device. b, The $V_{xxy}^{2\omega}$ signal as a function of the V_{xx}^{ω} at different temperatures from 100 to 300 K. c, The $V_{xxx}^{3\omega}$ signal as a function of the V_{xx}^{ω} at different temperatures from 100 to 300 K.

Supplemental Note 11: The $V_{xxx}^{3\omega}$ signal as a function of the V_{xx}^{ω} at different temperatures from 80 to 400 K.

The $V_{xxx}^{3\omega}$ increases with the decrease of temperature. It is noteworthy that the signal mutates at 300 K, which is precisely the ferromagnetic dependence of QMD described in the main text. The $V_{xxx}^{3\omega}$ above the Curie temperature is caused by the unavoidable disordered scattering of electrons due to the high conductivity in the Fe_5GeTe_2.

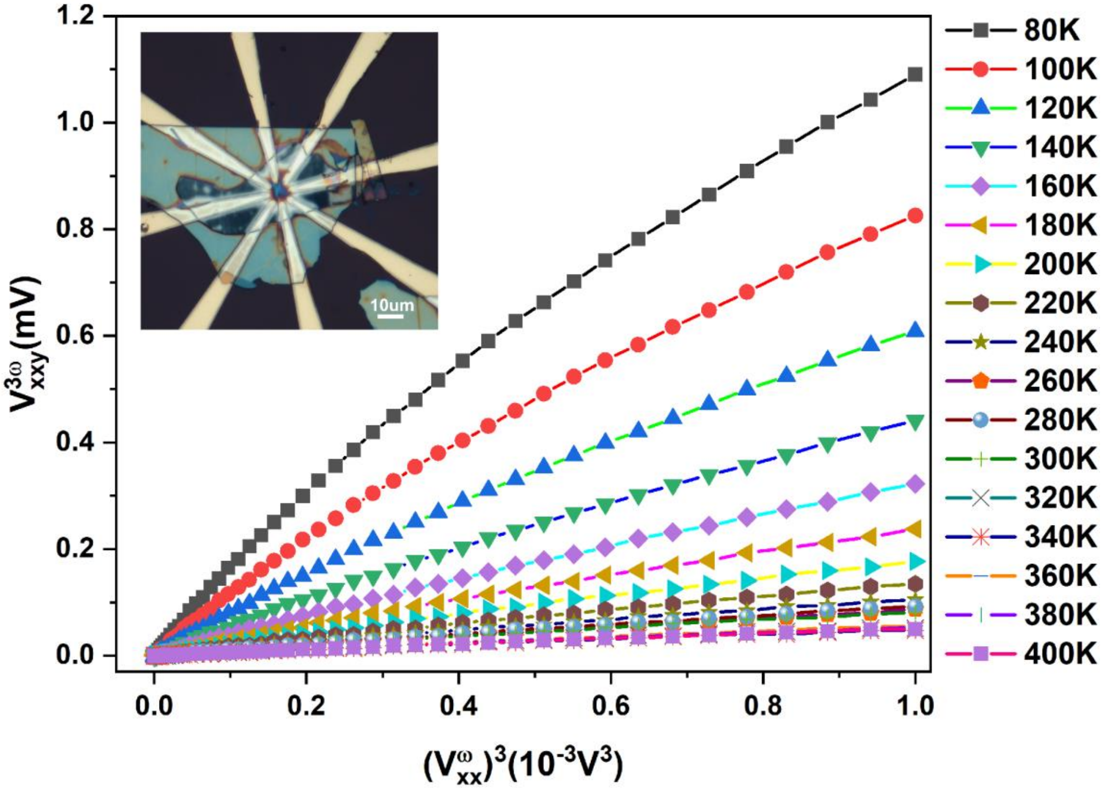

Supplementary Figure S12|The $V_{xxx}^{3\omega}$ signal as a function of the V_{xx}^{ω} at different temperatures from 80 to 400 K. In set: the optical microscope photograph of the device.

Supplemental Note 11: Nonlinear transport testing of Fe_5GeTe_2 device (> 100 nm) at temperatures range from 1.6 K to 300 K.

In order to further increase the upper limit of the observed temperature of $V_{xxx}^{3\omega}$ through the ferromagnetic dependence of QMD, we prepared 100 nm near-bulk (T_c = 310 K) devices. By fitting the curve, we obtained that η_2 =115 μm^3·S^{-1}·V^{-2} and η_0 =-6 μm·S·V^{-2}, which means the contribution of Drude scattering is dominant in the third-order nonlinear transport of 100 nm-Fe_5GeTe_2. Thicker samples may introduce more defects and impurities and resulting the transverse asymmetric scattering by effective spin–orbit coupling of the electron or impurity. This is also proved by Figure S13a, which is an order of magnitude smaller than that in Fig. 4a under the same test conditions.

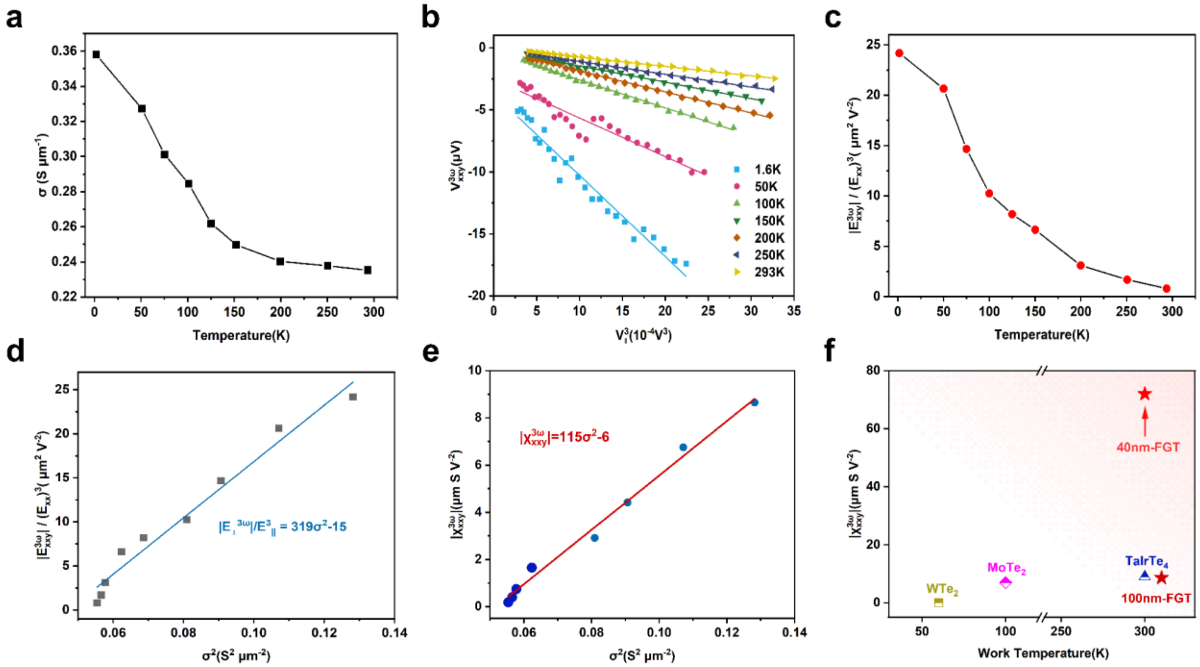

Supplementary Figure S13|Nonlinear transport testing of Fe_5GeTe_2 device (100 nm) at temperatures range from 1.6 to 300K. a, The longitudinal conductivity σ as a function of temperature. b, The $V_{xxy}^{3\omega}$ signal as a function of the $(V_{xx}^{\omega})^3$ at different temperatures from 1.6 to 300 K. c, The $|E_{xxy}^{3\omega}|/(E_{xx}^{\omega})^3$as a function of temperature. d, $|E_{xxy}^{3\omega}|/(E_{xx}^{\omega})^3$as a function of σ^2 in Fe_5GeTe_2. **e.** The scaling relationship between the third-order nonlinear conductivity $\chi_{xxy}^{3\omega}$ and the square of the linear longitudinal conductivity σ^2 The scaling is performed within the temperature range of 1.6-150 K. **f.** Comparison of the third-order nonlinear Hall conductivity and the operating temperature of different layers number Fe_5GeTe_2 with other materials.

References

(1) Kresse, G.; Furthmüller, J. Efficient iterative schemes for ab initio total-energy calculations using a plane-wave basis set. ***Phys. Rev. B*** 1996, 54, 11169.
(2) Blöchl, P. E. Projector augmented-wave method. Phys. Rev. B 1994, 50, 17953.
(3) Blöchl, P. E.; Jepsen, O.; Andersen, O. K. Improved tetrahedron method for Brillouinzone integrations. ***Phys. Rev. B*** 1994, 49, 16223.
(4) Perdew, J. P.; Burke, K.; Ernzerhof, M. Generalized gradient approximation made simple. ***Phys. Rev. Lett.*** 1996, 77, 3865.
(5) Togo, A.; Tanaka, I. First principles phonon calculations in materials science. ***Scr. Mater.*** 2015, 108, 1–5.